

Real-time tunable negative stiffness mechanical metamaterial

Xiaojun Tan^a, Shuai Chen^a, Bing Wang^{a,*}, Jie Tang^b, Lianchao Wang^a, Shaowei Zhu^a, Kaili Yao^a, Peifei Xu^a

^a National Key Laboratory of Science and Technology on Advanced Composites in Special Environment, Harbin Institute of Technology, Harbin 150080, PR China

^b School of Mechanics and Engineering, Southwest Jiaotong University, Chengdu 611756, PR China



ARTICLE INFO

Article history:

Received 27 December 2019

Received in revised form 7 September 2020

Accepted 16 September 2020

Available online 19 September 2020

Keywords:

Real-time tunable

Pneumatic actuation

Negative stiffness

Mechanical metamaterial

ABSTRACT

Real-time tunable mechanical metamaterial is an emerging field attracting great attention. It enables a wide range of mechanical properties but is hard to design and fabricate due to its complexity. Here, a pneumatically actuated tunable negative stiffness mechanical metamaterial with real-time tunable properties is presented. Numerical simulations and experiments were both employed to investigate the proposed real-time tunable negative stiffness mechanical metamaterial. Research results demonstrate that multistage pattern-transformation can be realized through the pneumatic actuation. Uniaxial compression and vibration tests reveal the influence of the inner air pressure on the metamaterial's basic mechanical properties and the vibration isolation performance, respectively. Additionally, real negative stiffness behavior and high energy absorption efficiency are achievable for the proposed metamaterial. This study can be a reference to relevant researches on tunable mechanical metamaterials, and presents a new path for designing real-time tunable negative stiffness mechanical metamaterials.

© 2020 Elsevier Ltd. All rights reserved.

1. Introduction

Mechanical metamaterials are of unusual mechanical properties through designing their cell structure rather than the chemical make-up [1,2]. The concept of metamaterials originated in the field of electromagnetic material [3], and has attracted great interests since its introduction to mechanics. To date, a considerable amount of literature about mechanical metamaterials has been published. The mechanical metamaterials can be divided into several types, including [1]: extremal materials [4], negative materials [5], ultra-property materials [6], and origami-based materials [7]. Negative stiffness (NS) mechanical metamaterials, investigated in this paper, belong to the negative materials, which also includes metamaterials with negative compressibility [8] and negative Poisson's ratio [9].

Negative stiffness is characterized by an increase in deformation resulting in a load drop [10]. Mechanisms with NS mechanical behavior have been already applied in the industrial fields, such as the field of MEMS (Micro Electro Mechanical Systems) [11] and vibration isolation [12]. Unlike the NS mechanisms [13], the NS mechanical metamaterial, consisting of periodic arrangement of NS elements, is an emerging field, which

gains increasing attention recently. The NS mechanical metamaterial can be generally divided into mono-stable [14–16] and multi-stable [5,17–21]. It can also be divided into compression induced [22,23], shear induced [5,24], twist and rotation induced [25–27] NS mechanical metamaterials according to the deformation modes. Certainly, NS mechanical metamaterials can be built with many kinds of NS elements, such as the curved beam element [10,23,28,29], magnets system [17,20], and shell elements [30,31]. The NS mechanical metamaterials have been proved to have great prospect in energy absorption [14,15,19,21,23,32,33], vibration isolation [34–36], advanced actuators [37], and deployable structures [18,19], owing to their unusual mechanical properties.

Real-time tunable mechanical metamaterial is an increasingly important topic in the field of metamaterials. It possesses a wide range of mechanical properties to deal with complex service environments. However, real-time tunable materials were rarely used in engineering field due to their complexity, cost, and power [38]. Recently, researchers have shown an increased interest in real-time tunable mechanical metamaterial because of the emergence of some new technologies, such as multi-material 3D printing and 4D printing [39]. Tunable property of current mechanical metamaterials mainly relied on the excitation from adsorptive physical fields. For instance, thermal activation was introduced to control the auxetic behavior of a mechanical metamaterial [40]. The thermal stimulus was also employed to shift the topology of

* Corresponding author.

E-mail address: wangbing86@hit.edu.cn (B. Wang).

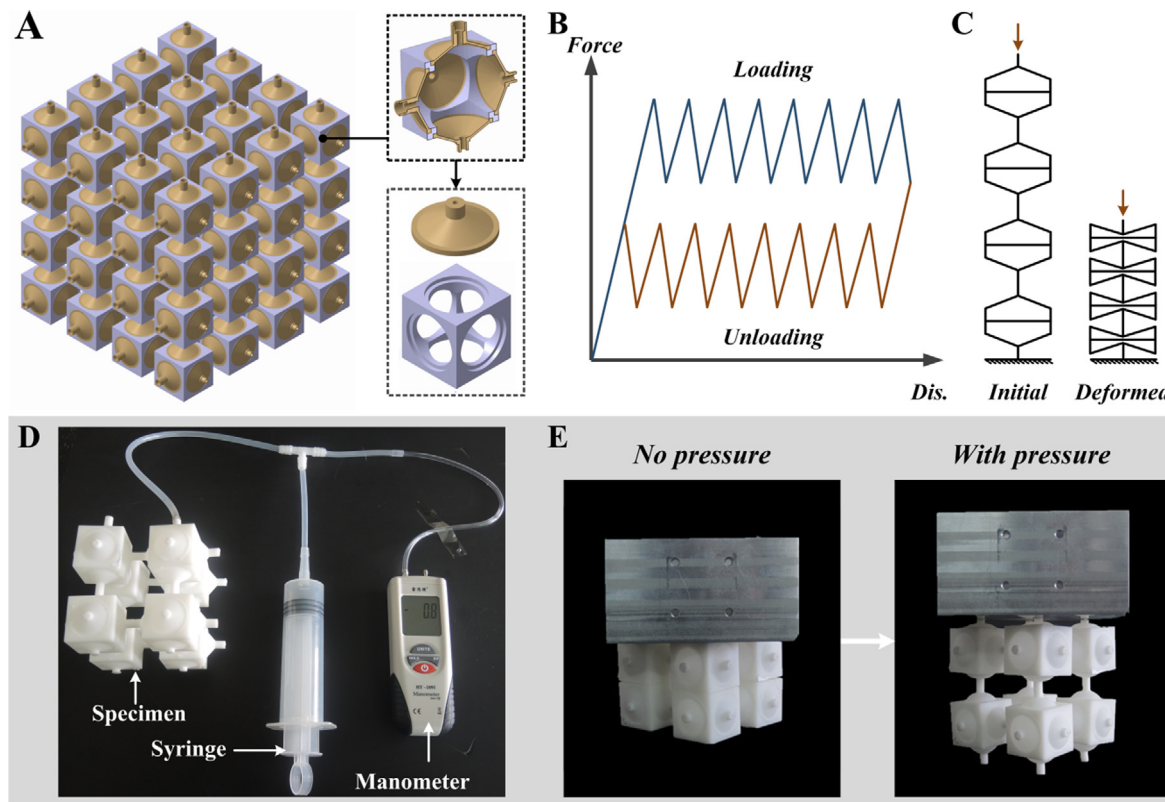


Fig. 1. (A) schematic diagram of tri-directional NS mechanical metamaterial and its details; (B) mechanical response diagram of metamaterial under loading–unloading condition; (C) Deformation mode of NS metamaterial under loading; (D) physical picture of real-time tunable NS mechanical metamaterial; (E) left picture, indicates that metamaterial is easy to collapse without effect of inner pressure; right picture, indicates that metamaterial is of good load-bearing capacity with effect of inner pressure.

a cellular solid between the bending-dominated and the stretch-dominated to tune the mechanical properties [41]. Additionally, mechanical [34,42] and magnetic [43] field are also the frequently used, alternative approaches to tune the properties of the mechanical metamaterials.

In terms of the tunable negative stiffness mechanical metamaterials, the relevant research is still in the initial stage, and only a small amount of literatures have been published recently. The mechanical excitation was the most frequently used method in these researches. Lateral confinement was applied to tune the response of a NS mechanical metamaterial to uniaxial compression [44]. Pre-compression was directly exerted on the beam element to design programmable NS mechanical metamaterials with tunable bandgap characteristics and stretchability [18]. Dynamic energy dissipation of the NS mechanical metamaterials was also tuned macroscopically through mechanical loading [34]. The method with mechanical fields are easy to implement, but is of low efficiency and non-real-time. Thus, it is necessary to design real-time NS mechanical metamaterial with some other tuning methods.

In this study, a NS mechanical metamaterial with real-time tunable properties via pneumatic actuation is presented and investigated. The work can be divided into following several parts. First, the geometries and the tuning method are introduced in detail. Then, numerical and experimental methods, used to characterize the proposed metamaterial, are introduced. Finally, the basic mechanical properties, energy absorption properties, and the vibration control properties of the real-time tunable NS mechanical metamaterials are studied and discussed.

2. Materials and methods

2.1. Materials and experiments

The proposed NS mechanical metamaterial, as shown in Fig. 1A, is composed of the NS conical shell elements and the cubic supporting structure. Its NS property has been studied in our previous research [30], and the research results suggested that the NS behavior was achievable in three dimensions. The diagrams of the metamaterial's response curve and deformation mode are displayed in Fig. 1B and C, respectively. Moreover, the energy absorption property of the metamaterials is tailorable by changing the medium density of the unit cell [30], which is a cavity, as displayed in Fig. 1A. In this paper, the characteristic of the metamaterial's architecture is further utilized to tune the mechanical properties. The physical picture of the real-time tunable NS mechanical metamaterial is illustrated in Fig. 1D. The real-time tunable mechanical metamaterial mainly consists of a pneumatic actuator, a manometer, and a specimen of the tri-directional NS mechanical metamaterial. A syringe is selected as the pneumatic actuator, and air pumps with higher driving efficiency can be introduced in practical application. The manometer (HT1890, Dongguan Xintai Instrument Co., Ltd) is for monitoring the inner pressure of the metamaterial.

The operation of tuning the metamaterial via pneumatic actuation is simple, but this efficient scheme proposes a special requirement for the metamaterial, i.e., the gas tightness of the metamaterial should be good. Complex sealing treatment was applied in some previous researches [45] to ensure the effectiveness of the pneumatic actuation. By contrast, it is unnecessary in this study because of the unique architecture of the presented NS mechanical metamaterial. Through tuning the inner pressure of

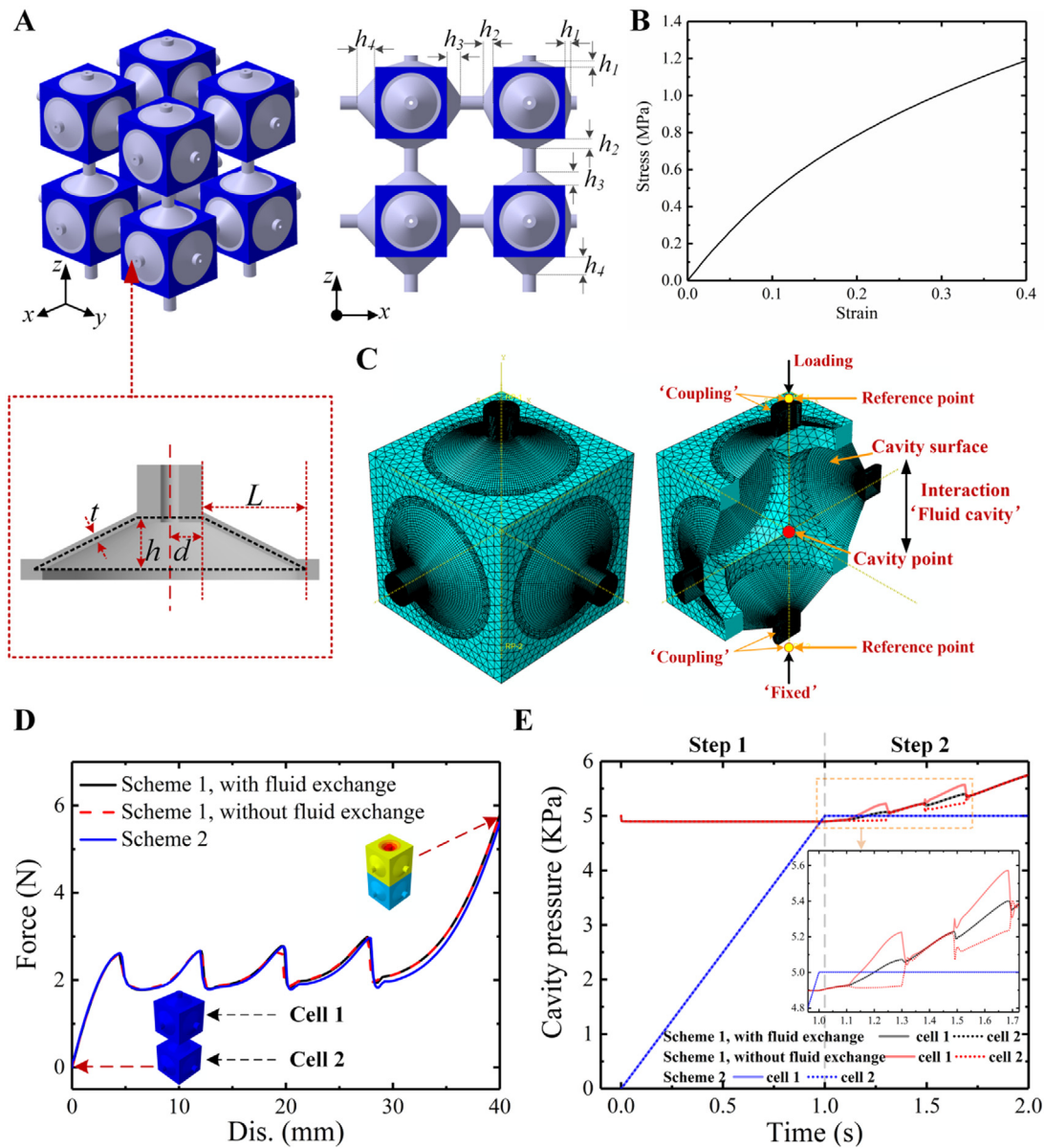


Fig. 2. (A) Geometries of tri-directional NS mechanical metamaterial; (B) true stress-strain response curve of shell element's base material; (C) FEM model of metamaterial's cell; (D) comparison of mechanical response of metamaterial with inner air pressure between different schemes of loading inner air pressure; (e) real-time inner air pressure of unit cells during loading process for different schemes of loading inner air pressure.

the metamaterial with a syringe, the metamaterial's mechanical properties can be changed in real-time. A simple experiment, as shown in Fig. 1E, can well demonstrate the tunable property of the proposed NS mechanical metamaterial with the pneumatic actuation. As we can observe, the metamaterial is of poor load-bearing capacity without the effect of inner air pressure, while this capacity improved a lot when with the input pressure through the pneumatic actuation.

The tri-directional NS mechanical metamaterial was fabricated with a combination of gel-casting method, stereo lithography appearance (SLA), and interlocking assembly method. The detailed fabrication process have been described in the previous literature [30]. The material parameters of the conical shell's base material were obtained via the standard tensile tests according to ASTM D638-14, and the true stress-strain response curve is displayed in Fig. 2B. The density of the conical shells' base material is 1200 kg/m^3 . The elastic modulus and the density

of the supporting structures are 2650 MPa , and 1100 kg/m^3 , respectively.

Two specimens with different geometries were selected for the experiment. The specimen 1 and specimen 2 were non-gradient and gradient structure, respectively, and the detailed geometries of the specimen were shown in Fig. 2A. The default parameters L , d , and t , as shown in Fig. 2A, for these two specimens were set as 10 mm, 3.5 mm, and 1 mm, separately. L and d represent the external and internal diameter of the truncated-conical shell element, and t is the thickness of the shell. The height, h , of the shell in specimen 1 is determined as 5 mm ($h_1 = h_2 = h_3 = h_4 = 5 \text{ mm}$), and the shell's height in specimen 2 was gradient, which increases from 3 to 9 with an increment of 2 mm along the axial directions ($h_1 = 3 \text{ mm}$, $h_2 = 5 \text{ mm}$, $h_3 = 7 \text{ mm}$, $h_4 = 9 \text{ mm}$).

Experiment setups for the quasi-static compression and vibration tests are introduced in Section 3.

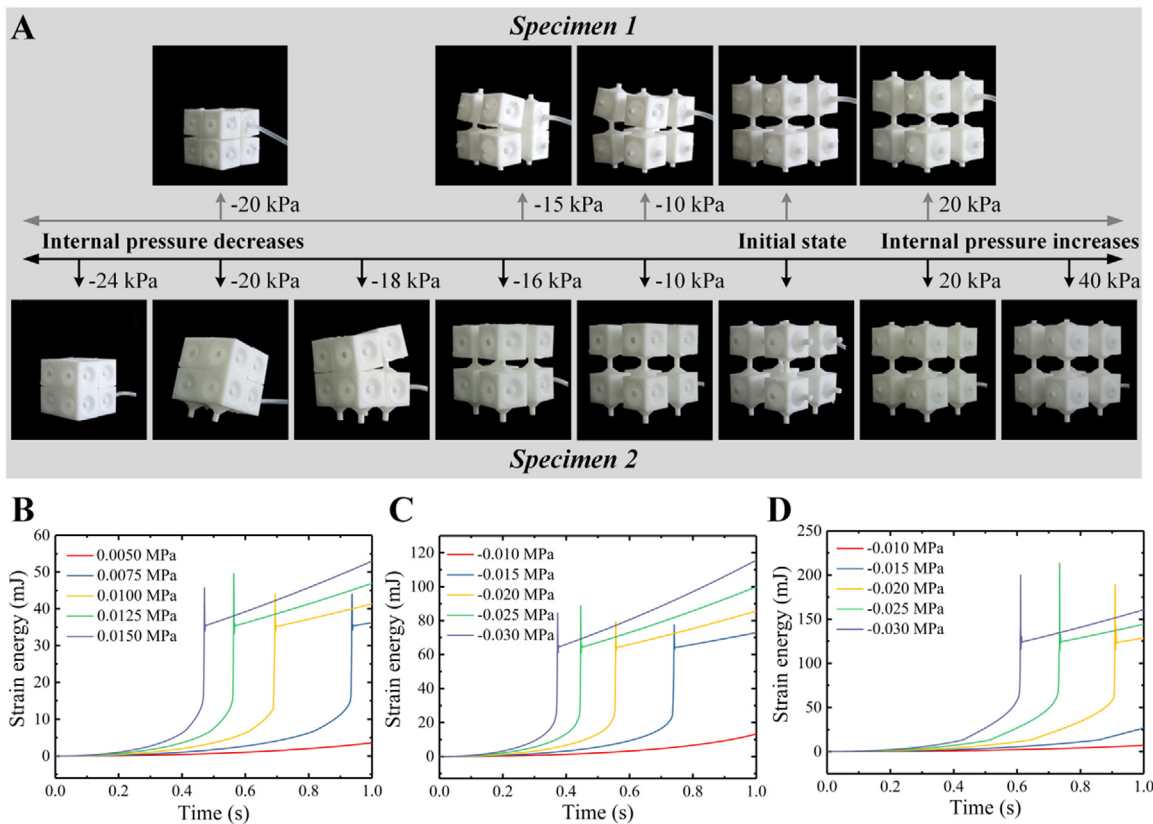


Fig. 3. (A) Deformation process of specimen 1 and specimen 2 under the effect of inner air pressure; (B) strain energy response of unit cell ($h = 5$ mm, $t = 0.8$ mm) as the deformation proceeds; (C) strain energy response of unit cell ($h = 5$ mm, $t = 1$ mm) as the deformation proceeds; (D) strain energy response of unit cell ($h = 7$ mm, $t = 1$ mm) as the deformation proceeds.

2.2. Numerical simulations

The numerical simulations were conducted with the commercial software ABAQUS and the FEM model of a real-time tunable NS mechanical metamaterial's unit cell is shown in Fig. 2C. The average element size of the conical shells and the supporting structure was respectively set as 0.25 mm and 2 mm to ensure the calculation efficiency and the correctness [30]. The shell element S4R (a general shell element with good adaptability, and it was applicable not only for the thick shells, but also for thin shells) was selected to mesh the conical shell structures through the 'Algorithm', 'Medial axis'. The cubic supporting structures were meshed with the element C3D4 due to its irregular shape. The conical shell structures and the supporting structures were assembled together through the interaction 'Tie' in ABAQUS. The true stress-strain response of the shells' base material was fitted via the 'Neo Hooke' Model in the 'Material Manager'.

In order to simulate the effect of the air pressure, one function in ABAQUS named 'Fluid cavity' was used, and one cavity point was created at the center of each unit cell. The surface of the conical shell element was defined as the cavity surface, which was interacted with the cavity point through 'Fluid cavity'. The 'Interaction', 'Fluid cavity', was defined in the 'Interaction Property Manager'. The characters of the 'Fluid cavity' were attributed to unit cells in the 'Create Interaction'. The 'Fluid cavity pressure' (inner air pressure) can be edited in the 'Boundary Condition' or in the 'Predefined Field Manager'. There are some differences between these two schemes of loading the 'Fluid cavity pressure'. If the 'Fluid cavity pressure' was loaded in the 'Predefined Field Manager' during the 'Initial step' (scheme 1), the metamaterial would deform with the effect of the inner pressure, which led to the increase or decrease of the defined cavity pressure. Thus

the defined pressure was not completely the same with the experiments, in which the defined inner pressure value reflected the state of the deformed metamaterial. This small difference may affect the mechanical response of the metamaterial. However, the advantages of this scheme were that the internal pressure was changing as the inner volume of the cavity changed, and the 'Fluid exchange' between cells can also be considered. If the 'Fluid cavity pressure' was loaded in the 'Boundary condition' (scheme 2), the inner pressure would remain constant as the compression on the metamaterial processed, which was inconsistent with the actual case. As we all know, the inner pressure would increase when the metamaterial under uniaxial compression, due to the decrease of the inner volume. Thus, this scheme may cause errors in the mechanical response of the metamaterial with the inner pressure.

Comparisons between these two schemes were made, and results were shown in Fig. 2D–E. Fig. 2D shows the compressive response of a structure (composed of two cells in series) with the inner air pressure. The inner air pressure of each cell was monitored, and was illustrated in Fig. 2E. In scheme 1, the inner air pressure of the cells decreased in the initial stage of the step 1, and then increased in step 2. During step 2, sharp decrease of the pressure happened because of the snap-through behavior. 'Fluid exchange' between each cell also had influence on the inner pressure. The inner pressure of each cell was always the same as the compression proceeded when the 'Fluid exchange' was considered, which was different from the case without the fluid exchange. Moreover, as we can see, the average pressure value of the two cells (without fluid exchange) equaled the pressure value of the cell (with fluid exchange). Moreover, in scheme 2, the internal pressure of the cell increased to the defined value in step 1, and then remained constant in Step 2.

The compressive response results of the different schemes were shown in Fig. 2D. Interestingly, the difference between these two schemes can almost be neglected. Only subtle differences existed in the latter part of response. The 'Fluid exchange' also had no influence on the mechanical response. These interesting conclusions were easy to explain. The volume of the cavity is large, the volume change caused by the deformation can be neglected, and thus difference between the scheme 1 and 2 in this case was very small. With a comprehensive consideration of the calculation efficiency and the accuracy, the scheme 2 was chosen in this manuscript.

In this paper, the deformation processes of the metamaterial under the negative and positive inner air pressure were both simulated in ABAQUS. Moreover, the compressive properties and the energy absorption property of the metamaterial with inner air pressure were also studied with numerical simulations. Different 'Steps' were employed in these different simulations. In the simulation of the deformation process of the metamaterial with negative inner air pressure, 'Dynamic explicit' was applicable. The 'Static, General', 'Dynamic explicit', and 'Dynamic, Implicit' step were all applicable for the simulation of the metamaterial with positive inner pressure, however, the 'Static, General' and the 'Dynamic, Implicit' were more effective. 'Dynamic, Implicit' was chosen to simulate the whole deformation process of the metamaterial under displacement controlled loading and loading-unloading. In the simulation of the compressive response of the metamaterial with positive inner pressure, the 'Fluid cavity pressure' was loaded in the step 1 ('static, general'), and then the displacement-controlled loading was exerted on the metamaterial in the step 2 ('Dynamic, Implicit'). In the step 2, the displacement controlled loading was exerted on the upper surface of the metamaterial, and the lower surface was fixed. The DOFs (degree of freedom) of the supporting structures were fixed, except the loading direction.

3. Results and discussion

Pattern-transforming of the proposed metamaterial, driven by the pneumatic actuator, was demonstrated through experiments, and the critical pressure was verified through the numerical simulations. The deformation process for the specimen 1 under pneumatic actuation is displayed in the upper half of Fig. 3A. As the inner pressure, controlled by the pneumatic actuator, increased, the metamaterial would swell (its dimension become larger). Moreover, the metamaterial would shrink to a contracted state with the decrease of the inner pressure. During the process, pattern-transformation happened and it was a dynamic process, which was hard to capture. However, the pressure range contained the critical pressure to the pattern-transformation can be determined through the observation of the deformation process. As can be seen from Fig. 3A, the significant deformation happened for the specimen 1 when the inner pressure decreased from -10 kPa to -15 kPa, and it can be inferred that most of the sub-elements transformed to another state during this process. The critical pressure to the pattern-transformation of the metamaterial varies in a range and was not an exact value due to the difference in each sub-element, caused by the fabrication error.

The critical pressure range estimated from the experiments was also verified through the numerical simulations. The details of the numerical method can be found in Section 2. Through the commercial software, ABAQUS, the pattern-transformation process of a unit cell was simulated, and the deformation processes were displayed in the upper part of Fig. 5A. The air pressure was exerted on the inside of the cell, and the cell would deform when the inner negative pressure was low. As the inner negative pressure increased, the pattern-transformation would happen.

The strain energy of a unit cell increased as the deformation proceeded when the pressure (-0.005 MPa) was low, demonstrated in Fig. 3B (the red curve). However, with high inner negative pressure, the strain energy would increase, and then drop suddenly during the deformation process, as shown in Fig. 3B. The sudden drop in strain energy was caused by the pattern-transformation process, during which some strain energy transformed to the kinetic energy. Response curves of strain energy for the unit cell with the same sub-element as the specimen 1 are displayed in Fig. 3C. The critical pressure to the pattern-transformation is in the range from -10 kPa to -15 kPa (-15 kPa \leq critical pressure < -10 kPa), which was almost identical with the experiment results. The comparison of critical pressure between experiments and simulations proved the effectiveness of the experiment and the correctness of the numerical methods.

The deformation process of the gradient metamaterial, specimen 2, under pneumatic actuation was also demonstrated through experiments, and was displayed in the bottom half of Fig. 3A. The deformation mode of the gradient metamaterial was similar to that of the specimen 1 when the inner air pressure was positive. However, a significant difference would appear when the inner pressure turned negative. As displayed in Fig. 3A, the gradient metamaterial's upper layer snapped to another pattern as the pressure varied from 0 kPa to -10 kPa. The pattern-transformation of the gradient metamaterial exhibited obvious gradualness from the initial to the contracted state as the inner pressure decreased from 0 kPa to -24 kPa, and this multistage pattern-transformation may have application potential in deployable space structure. Generally, it can be concluded that the pattern-transformation can be triggered through the pneumatic actuation, and the process can be tuned through structural design, such as the gradient design.

The relationship between the geometric parameters and critical pressure to the pattern-transformation was preliminarily studied. The response curves of the strain energy for different cell under various negative inner pressures were simulated and illustrated in Fig. 3B-D. The parameter h and t for the specimen, whose responses were illustrated in Fig. 3B, were 5 mm and 0.8 mm, respectively. The parameter h and t for the specimen, whose responses were illustrated in Fig. 3C, were 5 mm and 1 mm, respectively. The parameter h and t for the specimen, whose responses were illustrated in Fig. 3D, were 7 mm and 1 mm, respectively. These three specimens processed the same internal diameter, $d = 3.5$ mm, and the external diameter, $L = 10$ mm. As can be observed from Fig. 3 B-D, the negative critical pressure ranges to the pattern transformation for these specimens were 5 kPa-7.5 kPa, 10 kPa-15 kPa, and 15 kPa-20 kPa, separately. The critical pressure range increased as the height or the thickness of the shell element increased. This may partly be explained by the relationship between the element's strength and the geometric parameters, which has been demonstrated in the previous research [30], i.e., increasing the shell element's height and thickness can improve its strength.

The deformation (shrink) processes of the metamaterials (specimen 1, $2 \times 2 \times 2$ and $3 \times 3 \times 3$) under the negative inner pressure (-20 kPa) were also simulated in ABAQUS. The simulation results were shown in Fig. 4. As can be observed, the metamaterial shrank from the initial state to the contracted state gradually, which was consistent with the experiments. Moreover, it can also be found that the conical shells in the metamaterial did not collapse simultaneously, which was more obvious in the deformation process of the metamaterial ($3 \times 3 \times 3$). Combining the experiment and numerical results, it can be concluded that it was hardly possible for the conical shells in the metamaterial to collapse simultaneously when under the negative inner pressure, which was attributed to the fabrication errors and the interaction between cells.

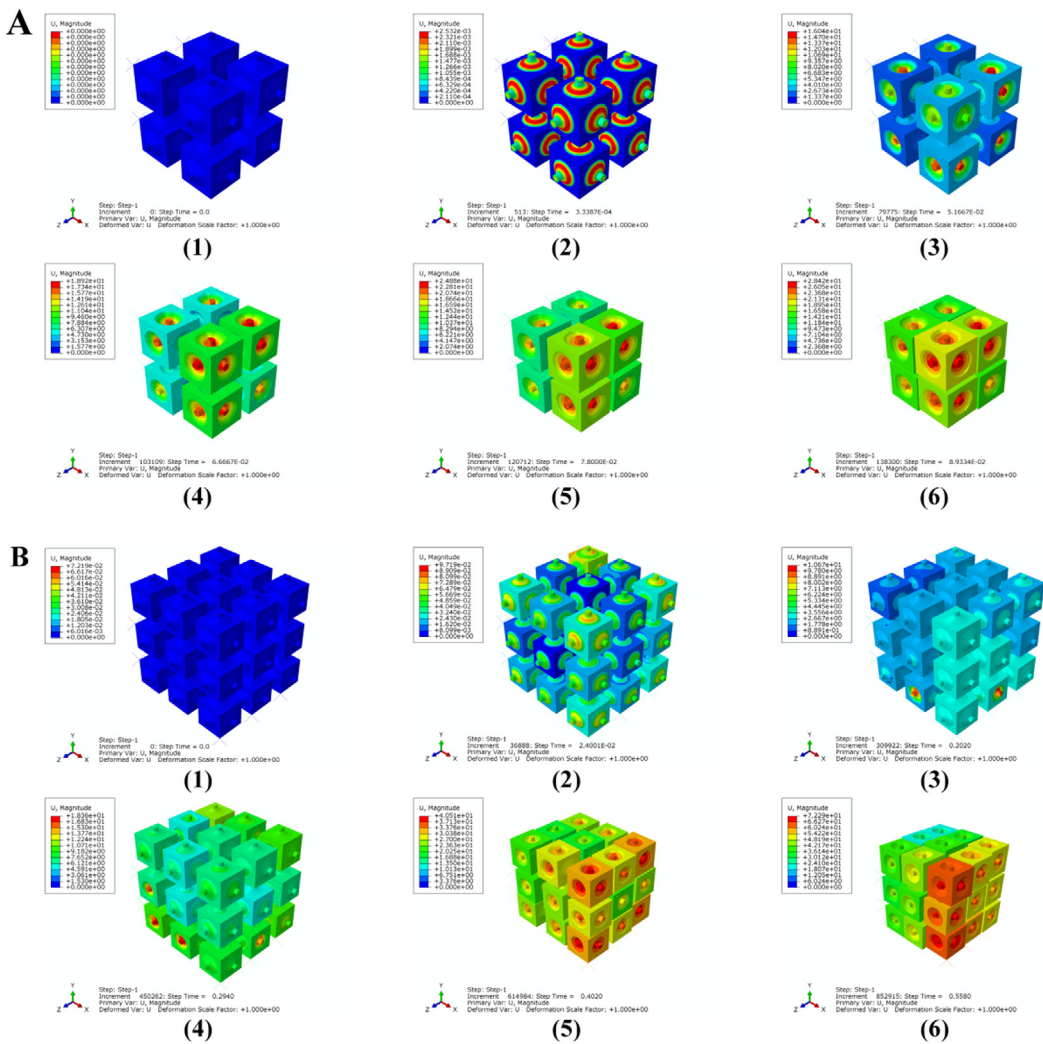


Fig. 4. Deformation processes of metamaterials under negative inner pressure (-20 kPa): (A) specimen 1 (metamaterial $2 \times 2 \times 2$); (B) metamaterial ($3 \times 3 \times 3$).

The tunable mechanical response of the metamaterial under uniaxial compression was also demonstrated through both experiments and simulations. The simulation process from the initial state to the deformed state under uniaxial loading is displayed in the bottom half of Fig. 5A, and should be divided into two steps. During the first step, pre-deformation was applied through the pneumatic actuator, and the cell swelled or shrank. Then the uniaxial displacement controlled loading was exerted on the cell. The experiment setup was shown in Fig. 5B, and the geometric parameters of the selected cell were same as those of the specimen 1.

The force-displacement responses of the unit cell with the effect of different inner pressure were illustrated in Fig. 5C–D. The results from experiments and simulations were also compared. The responses of the NS unit cell with the inner air pressure equaling 0, 5, 10, 15, and 20 kPa were studied. As we can observe, the results from experiments and simulation showed reasonable agreement for each condition, which further verified the correctness of the numerical methods. Additionally, these two graphs showed that there was a slight increase in the strength, while the initial stiffness almost remained steady as the inner pressure increased. The negative stiffness behavior weakened gradually with the increment of the positive pressure, and exhibited a long plateau, which indicated the potential of the real-time tunable metamaterial in energy absorption.

The tunable compressive responses of the metamaterials (specimen 1, $2 \times 2 \times 2$, $3 \times 3 \times 3$) were also studied via numerical simulations. The loading processes, including the inner air pressure and uniaxial displacement loading, were shown in Fig. 6A–B. The mechanical response curves of the metamaterials ($2 \times 2 \times 2$ and $3 \times 3 \times 3$) were displayed in Fig. 6 C–D. The phenomenon observed in Fig. 6 C–D was consistent with that in Fig. 5 C–D. The metamaterials ($2 \times 2 \times 2$ and $3 \times 3 \times 3$) also exhibited a long plateau when the inner air pressure equaled 10 kPa. Moreover, the peaks, corresponded to the unstable buckling of the conical shell element, in response curves disappeared gradually as the positive air pressure increased, and the serrated response curves eventually turned to the curves, which was monotone increasing. In our opinion, the peaks disappear due to the influence of the positive air pressure. The inner positive pressure acts like a positive stiffness spring. When a negative stiffness element was assembled with a positive stiffness spring, the quasi-zero stiffness response can be obtained (like the red response curve in Fig. 6 C–D). As the positive pressure continually increased, the assembled structure would exhibit positive stiffness (like the gray response curve in Fig. 6 C–D), and the peaks would disappear.

The mechanical responses of a unit cell with the effect of negative air pressure were shown in Fig. 5E. The cells with the inner pressure equaling -10 kPa and -11 kPa were studied. It was important to note that these two pressure values did not reach the critical point to the pattern-transformation. It can

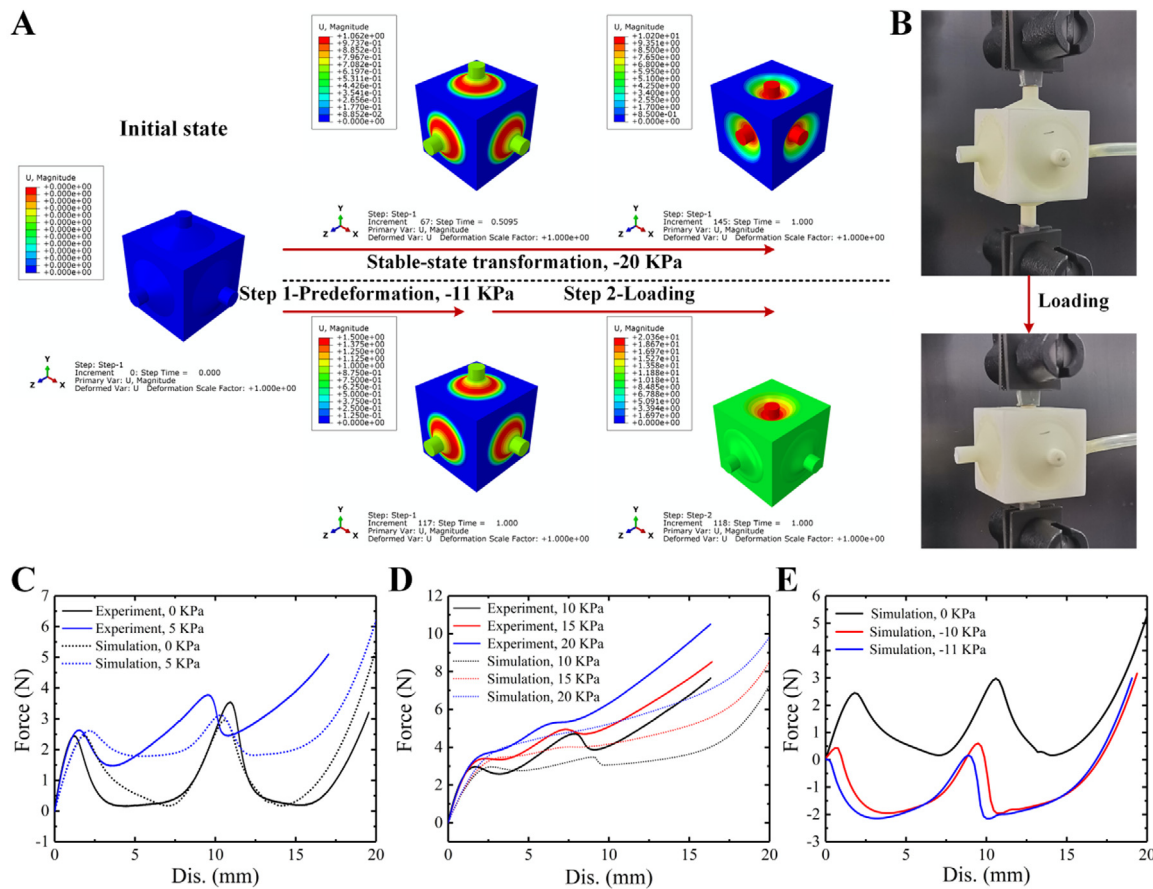


Fig. 5. (A) Up, pattern-transformation of metamaterial in simulation; down, simulation process of metamaterial with effect of inner pressure when under compression; (B) Experiment setups for metamaterial under compression; (C–D) force–displacement responses for metamaterial with effect of different positive pressure when under compression; (E) force–displacement responses for metamaterial with effect of different negative pressure when under compression;.

be seen from Fig. 5E that the initial positive stiffness region narrowed as the inner air pressure decreased, and almost disappeared when the pressure reached -11 kPa. According to the previous research [46], almost all current NS metamaterials were pseudo negative stiffness, because of the existence of the initial positive stiffness. In this paper, the initial positive stiffness region nearly disappeared with the effect of air pressure, as shown in Fig. 5E. Moreover, a completely real negative stiffness behavior is achievable in theory when the balance between the air pressure and structural stress is struck. Thus, the real-time tunable NS mechanical metamaterial in this study presented a new possible path for designing real NS metamaterials.

The NS mechanical metamaterial has great potential in energy absorption mainly due to its tailororable and extreme energy absorption efficiency. As shown in Fig. 7A, the force–displacement response exhibits a long, serrated, plateau, suggesting high energy absorption efficiency. However, this high efficiency is hugely dependent on the number of NS element in series. The efficiency drops sharply as the element's number decreases, and approaches zero when the number equals one or two [23,47,48]. This limit of NS metamaterial was proved through simulations. As shown in Fig. 7B, the mechanical response of a single unit cell under loading–unloading test was displayed, and it can be seen that the loading response and the unloading response were completely coincided with each other, which indicated that no energy was dissipated during this process. If more unit cells are arranged in series, the mechanical response would change. Mechanical response and simulation process of a NS structure with three cells in series was shown in Fig. 7C and G, respectively. It can be seen that some energy was dissipated during the loading–unloading

test. The dissipated energy can be obtained by calculating the area enclosed by the loading–unloading response curves. As the number of the unit cells in series increased, the energy absorption efficacy would increase, and the ideal response was shown in Fig. 7A. This limit (energy absorption was dependent on the number of cells in series) may restrict the development and NS metamaterials.

Here, this dependence can be overcome through our presented real-time tunable NS mechanical metamaterial. As demonstrated in Fig. 7H–I, the inner pressure of the metamaterial was set to positive (step 1) through pneumatic actuation when under loading (step 2), and the mechanical response curve was expected to be a long plateau like the response in Fig. 7A. Tuning the inner air pressure to negative once the metamaterial was compacted (step 3), and the metamaterial would remain deformed when unloading (step 4). The input mechanical energy would be locked as the strain energy with the rational pressure setting, and the mechanical response can be demonstrated by Fig. 7D, which exhibit high energy absorption efficiency, independent on the element number in series. Simulations were conducted to prove the concept above. The loading–unloading processes in ABAQUS were shown in Fig. 7I. With the tuning scheme, shown in Fig. 7H, the mechanical response curves of a single unit cell and a structure (three cells in series) were shown in Fig. 7E and F, respectively. It can be seen that the loading response exhibits long a long plateau, and the unloading response equaled 0 N through tuning the air pressure. Response curves in Fig. 7E–F well proved our assumption. The core of above concept is to load rational positive cavity pressure during loading process to construct the long plateau, and load rational negative cavity

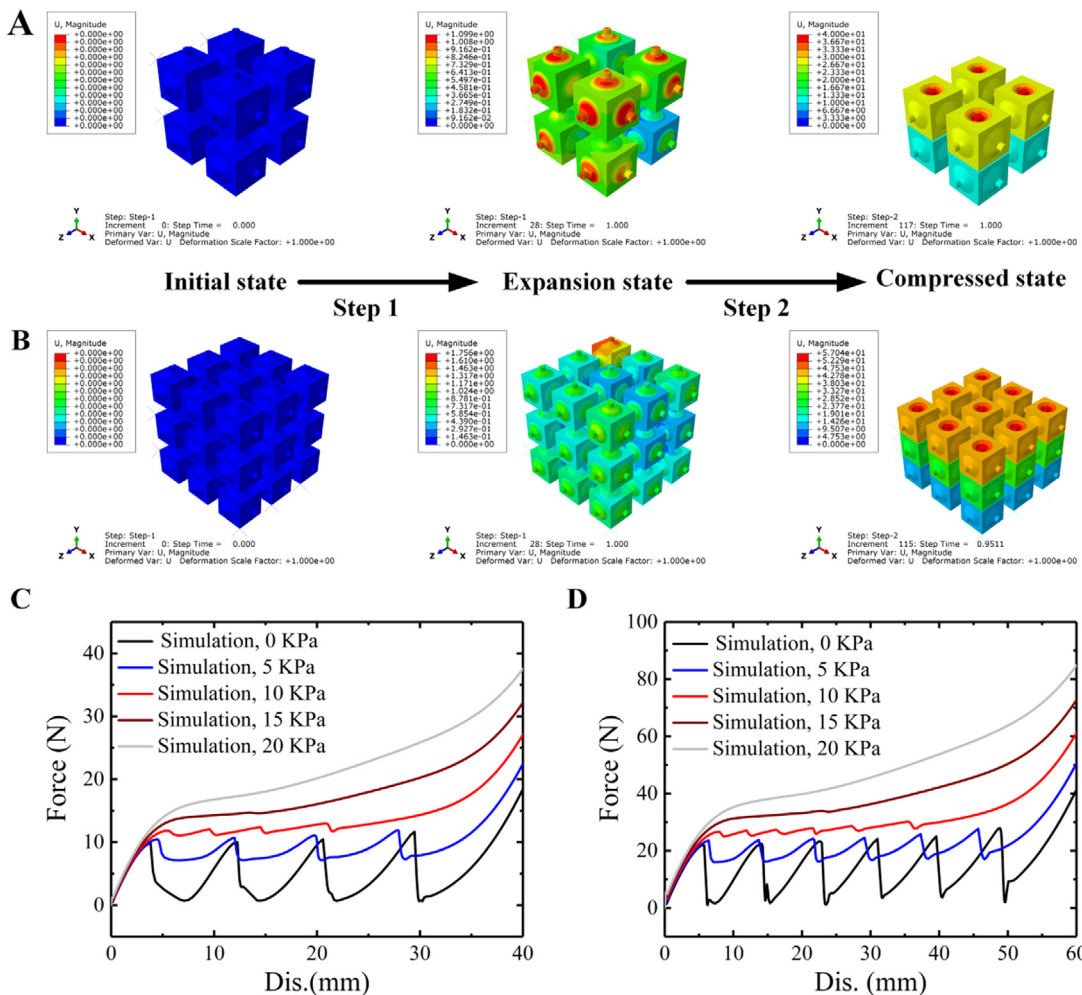


Fig. 6. Simulation processes of metamaterials with effect of positive inner pressure when under compression: (A) metamaterial ($2 \times 2 \times 2$); (B) metamaterial ($3 \times 3 \times 3$). Force-displacement response curves for metamaterial with effect of different positive inner pressure when under compression: (C) metamaterial ($2 \times 2 \times 2$); (D) metamaterial ($3 \times 3 \times 3$).

pressure to keep the metamaterial remain the deformed state during unloading step. In general, the high energy absorption efficiency can be achieved for the presented real-time tunable NS mechanical metamaterial through tuning the inner pressure instead of increasing the element's number.

The tunable property of the presented metamaterial also reflects in the vibration isolation performance. The influence of the inner pressure exerted with the pneumatic actuation on vibration isolation performance was studied with experiments, and the partial results were verified through the numerical simulation. The resonance frequency and vibration transmissibility of the metamaterial were tested to characterize the vibration isolation performance. The experiment setups, displayed in Fig. 8A, including the shaker table (DC-200-21, produced by Suzhou Sushi Experiment Group Co., Ltd.), the fixture, and the accelerometers (CA-YD-186, IEPE, produced by SINOCERA PIEZOTRONICS.INC.). The metamaterial was fixed on the lower fixture, and the upper fixture was bolted with metamaterial to enable the accelerometer can be fixed at the top center. Two accelerometers were fixed on the lower and upper fixtures, respectively, to monitor the input acceleration response of the shaker table and the output acceleration response. The shaker table excited the metamaterial from 20 Hz to approximately 300 Hz. The first resonance peak of each specimen was included in this range. The input acceleration a_{in} equaled 0.3 m/s [2]. The transmissibility was calculated through

the following formula:

$$T = \log_{10} \frac{|a_{out}|}{|a_{in}|}$$

where a_{out} was the output acceleration response. In the simulation of the metamaterials' resonance frequency, the 'Fluid cavity pressure' was firstly loaded on the cells of the metamaterials (Step 1), and then the 'Step', 'Frequency' was employed to calculate the resonance frequency (Step 2).

The frequency response curves for the gradient specimen 2 under the effect of positive and negative air pressure are illustrated in Fig. 8C and D, respectively. As observed from Fig. 8C, the resonance peak shifted to the lower frequencies with the increase of the positive pressure. However, the resonance peak shifted to the higher frequencies as the inner negative pressure decreased in general. In order to facilitate the observation and analysis, the resonance frequency and transmissibility of each curve in Fig. 8C-D were extracted, and displayed in Fig. 8E. It can be seen from the figure that the resonance frequency to the initial state was 52.5 Hz, which was close to the fundamental frequency from numerical result, 55.3 Hz, in Fig. 8I. As the inner pressure decreased from 0 to -20 kPa, the resonance frequency and the transmissibility both dropped, which could be explained by the pattern-transformation of the metamaterial. During this transformation, the metamaterial changed from the initial to the contracted state, and its dimensions varied significantly. With the

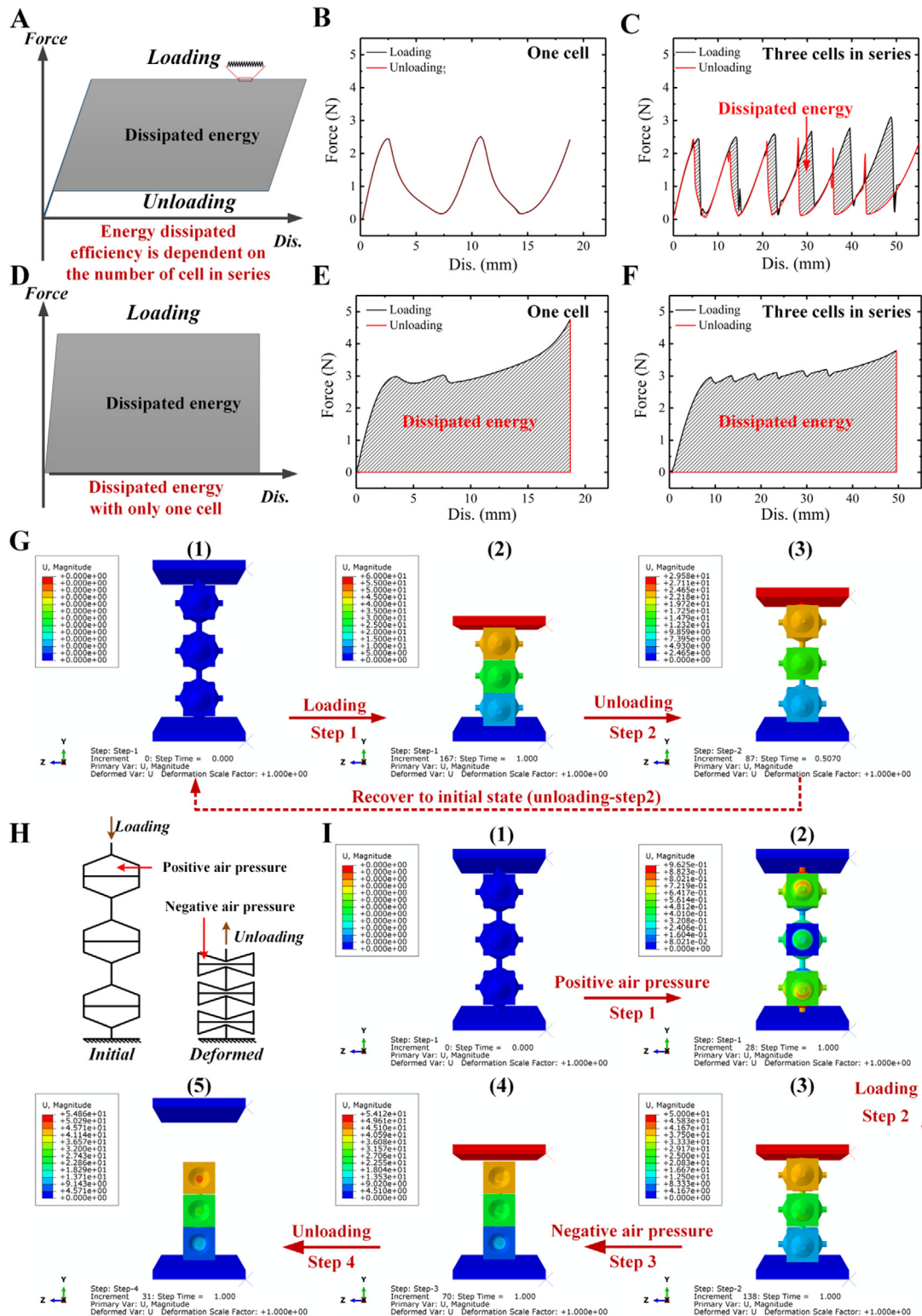


Fig. 7. (A) response diagram for NS metamaterial (many cells in series) under loading–unloading test; (B–C) response curve for NS structure (one cell) and NS structure (three cells in series) under loading–unloading test; (D) response diagram for presented tunable metamaterial under loading–unloading test; (E–F) response curve for metamaterial (one cell) and metamaterial (three cells in series) under loading–unloading test when with influence of inner pressure; (G) loading–unloading process for NS structure (three cells in series); (H) tuning scheme for presented metamaterial to improve energy absorption efficiency; (I) loading–unloading process for NS structure (three cells in series) when with influence of inner pressure.

gradual decrease of the pressure, the resonance frequency and the transmissibility both increased. A possible explanation for this trend might be that the cubic, supporting structure connected

with each other as the metamaterial contracted, and the metamaterial tended to be a rigid body, which further led to the increase of the resonance frequency and the transmissibility.

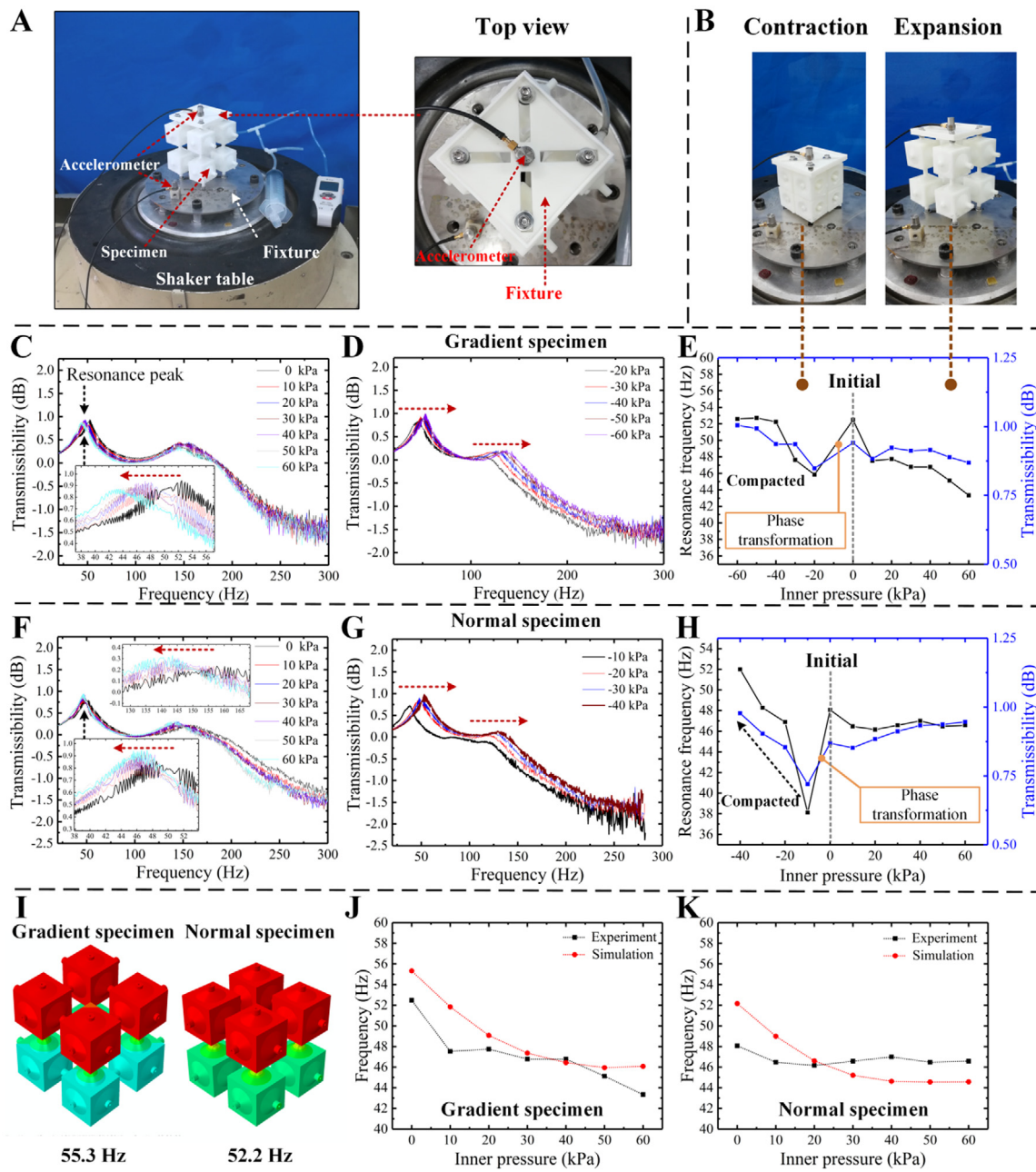


Fig. 8. (A) Experiment setups for the vibration testing; (B) contraction and expansion state of specimen 2 under the effect of inner pressure; (C–D) frequency response curve for gradient specimen with effect of: different positive pressure and different negative pressure; (E) relationship between inner pressure and resonance frequency and between inner pressure and transmissibility for specimen 2. (F–G) frequency response curve for normal specimen with the effect of: different positive pressure and different negative pressure; (H) relationship between inner pressure and resonance frequency and between inner pressure and transmissibility for specimen 1; (I) first-order modal from simulation for gradient specimen and normal specimen. Comparison results of resonance frequency between experiments and simulations: (J) gradient specimen; (K) normal specimen.

Additionally, Fig. 8E revealed that there has been a steady decline in the resonance frequency as the inner pressure increased from 0 kPa to 60 kPa, while the change of the transmissibility was not obvious. The phenomenon (i.e., the resonance frequency decreased as the positive inner pressure increased) was mainly caused by the fluid–structure interaction in the metamaterials. In the past study [49,50] of the influence of the internal fluid pressure on the hemispherical shell’s fundamental frequency, it has been proved that the fluid–structure interaction may even-tuate modal shape transformation and decrease the frequency. Moreover, as the inner air pressure increased, the mass of the metamaterial would increase, which may decrease the resonance frequency.

In order to verify the correctness of the above conclusion, the frequency response curves for the normal one, specimen 1, under the effect of positive and negative air pressure were also tested, and illustrated in Fig. 8F–G. The resonance frequency and the transmissibility for each condition were also extracted, and illustrated in Fig. 8H. It can be seen from the figure that the relationship between the inner pressure and the vibration isolation performance for the specimen 1 was almost consistent to that of specimen 2. Thus, it can be concluded that the influence of the inner pressure on the vibration isolation performance is common for the metamaterial in this paper, and the corresponding law summarized above is correct.

The resonance frequencies of the metamaterials with positive inner air pressure were simulated in ABAQUS to further verify the experiment results. The comparison results for the gradient specimen and the normal specimen were shown in Fig. 8J and K, respectively. It can be seen that the resonance frequency from simulation showed good agreement with the experiment results for the metamaterial with different positive pressure. The comparison results indicated that the experiments are reasonable.

One interesting finding in Fig. 8E and H was that the resonance frequency and the transmissibility both declined with the pattern-transformation. The transmissibility of the gradient specimen 2 decreased from 0.941 dB to 0.848 dB, with the change ratio of 9.85%. The resonance frequency decreased from 52.5 Hz to 45.9 Hz, with the change ratio of 12.6%. The change ratio for the specimen 1 in transmissibility and resonance frequency were 17.07% and 20%, respectively, when the pattern-transformation happened. Considering that the resonance frequency and transmissibility for the metamaterial at the initial state were very low, the change in vibration isolation performance, caused by pattern transformation, was still obvious. This real-time tunable property in vibration isolation performance has great application potential in engineering industry.

4. Conclusion

In this paper, a novel real-time tunable NS mechanical metamaterial is introduced and studied. The metamaterial is tuned through pneumatic actuation without further sealing treatment compared with similar metamaterials due to its unique cavity architecture. Experiments and numerical simulation were both employed to demonstrate the metamaterial's tunable property. Research results suggest that the pattern-transformation can be actuated through the pneumatic actuator, and the gradient metamaterial can exhibit gradual pattern-transformation. The inner positive pressure, controlled by the pneumatic actuator, has remarkable influence on the strength of the metamaterial, but has little influence on its initial stiffness. Moreover, the high energy absorption efficiency without dependence on the element's number and the real negative stiffness behavior are achievable through the rational pressure control. Additionally, the vibration isolation performance can be changed via tuning the inner pressure, and the pattern-transformation can be used to tailor the resonance frequency and transmissibility.

The concept of the real-time tunable NS mechanical metamaterial presented in this paper is highly original. Also this study systematically investigated the change law of the metamaterial's mechanical properties under the effect of the tuning device. Main conclusions drawn in this paper are all verified with a combination of experiments and numerical simulations, which ensure the correctness. However, some limitations do exist in this study. The main weakness of the study was that the efficiency of the tuning device, a pneumatic actuation, was not quantitatively measured, and the actuator was replaced with a syringe. Although the real-time tuning process can be actuated with the syringe, its efficiency still needs further improvement.

In order to overcome the limit in this study, an electric air pump can be introduced to replace the syringe to improve the efficiency. Moreover, PLC (Programmable Logic Controller) and some sensors can be applied for further design of self-sensing and self-tuning metamaterials.

Declaration of competing interest

The authors declare that they have no known competing financial interests or personal relationships that could have appeared to influence the work reported in this paper.

Acknowledgments

The present work is supported by National Natural Science Foundation of China under Grant No. 11972008, Natural Science Foundation of Heilongjiang Province, China under Grant No. A2018005, and Innovation Project of New Energy Vehicle and Intelligent Connected Vehicle, China. This paper is dedicated to the 100th anniversary of Harbin Institute of Technology, China. Congratulations.

References

- [1] A.A. Zadpoor, Mechanical meta-materials, *Mater. Horiz.* 3 (2016) 371–381.
- [2] A. Rafsanjani, D. Pasini, Bistable auxetic mechanical metamaterials inspired by ancient geometric motifs, *Extreme Mech. Lett.* 9 (2016) 291–296.
- [3] D.R. Smith, W.J. Padilla, D.C. Vier, S.C. Nemat-Nasser, S. Schultz, Composite medium with simultaneously negative permeability and permittivity, *Phys. Rev. Lett.* 84 (2000) 4184.
- [4] C.N. Layman, C.J. Naify, T.P. Martin, D.C. Calvo, G.J. Orris, Highly anisotropic elements for acoustic pentamode applications, *Phys. Rev. Lett.* 111 (2013) 024302, <http://dx.doi.org/10.1103/PhysRevLett.111.024302>.
- [5] X. Tan, et al., Novel multi-stable mechanical metamaterials for trapping energy through shear deformation, *Int. J. Mech. Sci.* 164 (2019) 105168, <http://dx.doi.org/10.1016/j.ijmecsci.2019.105168>.
- [6] X. Zheng, et al., Ultralight, ultrastiff mechanical metamaterials, *Science* 344 (2014) 1373–1377, <http://dx.doi.org/10.1126/science.1252291>.
- [7] E.T. Filipov, M. Redouey, Mechanical characteristics of the bistable origami hyspar, *Extreme Mech. Lett.* 25 (2018) 16–26, <http://dx.doi.org/10.1016/j.eml.2018.10.001>.
- [8] J. Qu, A. Gerber, F. Mayer, M. Kadic, M. Wegener, Experiments on Metamaterials with negative effective Static Compressibility, *Phys. Rev. X* 7 (2017) <http://dx.doi.org/10.1103/PhysRevX.7.041060>.
- [9] R. Lakes, Foam Structures with a Negative Poisson's Ratio, *Science* 235 (1987) 1038–1040.
- [10] X.J. Tan, et al., Reusable metamaterial via inelastic instability for energy absorption, *Int. J. Mech. Sci.* 155 (2019) 509–517, <http://dx.doi.org/10.1016/j.ijmecsci.2019.02.011>.
- [11] M.R. Brake, et al., Modeling and measurement of a Bistable Beam in a Microelectromechanical System, *J. Microelectromech. Syst.* 19 (2010) 1503–1514.
- [12] T.D. Le, K.K. Ahn, Experimental investigation of a vibration isolation system using negative stiffness structure, *Int. J. Mech. Sci.* 70 (2013) 99–112.
- [13] B. Haghpanah, A. Shirazi, L. Salari-Sharif, A. Guell Izard, L. Valdevit, Elastic architected materials with extreme damping capacity, *Extreme Mech. Lett.* 17 (2017) 56–61, <http://dx.doi.org/10.1016/j.eml.2017.09.014>.
- [14] X.J. Tan, B. Wang, S. Chen, S.W. Zhu, Y.G. Sun, A novel cylindrical negative stiffness structure for shock isolation, *Compos. Struct.* 214 (2019) 397–405, <http://dx.doi.org/10.1016/j.compstruct.2019.02.030>.
- [15] T. Frenzel, C. Findeisen, M. Kadic, P. Gumbsch, M. Wegener, Tailored Buckling microlattices as reusable Light-Weight Shock Absorbers, *Adv. Mater.* 28 (2016) 5865–5870.
- [16] A. Rafsanjani, A. Akbarzadeh, D. Pasini, Snapping Mechanical Metamaterials under Tension, *Adv. Mater.* 27 (2015) 5931.
- [17] X.J. Tan, et al., Design, fabrication, and characterization of multistable mechanical metamaterials for trapping energy, *Extreme Mech. Lett.* 28 (2019) 8–21, <http://dx.doi.org/10.1016/j.eml.2019.02.002>.
- [18] X. Tan, et al., Programmable Buckling-based negative stiffness metamaterial, *Mater. Lett.* (2019) 127072, <http://dx.doi.org/10.1016/j.matlet.2019.127072>.
- [19] B. Haghpanah, L. Salari-Sharif, P. Pourrjab, J. Hopkins, L. Valdevit, Multi-stable Shape-Reconfigurable architected materials, *Adv. Mater.* 28 (2016) 7915–7920.
- [20] T.A. Hewage, K.L. Alderson, A. Alderson, F. Scarpa, Double-negative mechanical metamaterials displaying Simultaneous negative Stiffness and negative Poisson's Ratio properties, *Adv. Mater.* 28 (2016).
- [21] S. Shan, et al., Multistable Architected Materials for trapping Elastic strain Energy, *Adv. Mater.* 27 (2015) 4296–4301.
- [22] D.M. Correa, et al., Negative stiffness honeycombs for recoverable shock isolation, *Rapid Prototyp. J.* 21 (2015) 193–200.
- [23] D. Restrepo, N.D. Mankame, P.D. Zavattieri, Phase transforming cellular materials, *Extreme Mech. Lett.* 4 (2015) 52–60.
- [24] S. Liu, A.I. Azad, R. Burgueño, Architected materials for tailorable shear behavior with energy dissipation, *Extreme Mech. Lett.* 28 (2019) 1–7, <http://dx.doi.org/10.1016/j.eml.2019.01.010>.
- [25] H.Y. Jeong, et al., 3D printing of twisting and rotational bistable structures with tuning elements, *Sci. Rep.* 9 (2019) 324, <http://dx.doi.org/10.1038/s41598-018-36936-6>.

- [26] Y. Zhang, Q. Wang, M. Tichem, F. van Keulen, Design and characterization of multi-stable mechanical metastructures with level and tilted stable configurations, *Extreme Mech. Lett.* (2019) 100593, <http://dx.doi.org/10.1016/j.eml.2019.100593>.
- [27] S. Zhu, et al., Quasi-All-Directional Negative Stiffness Metamaterials based on negative rotation Stiffness Elements, *Phys. Status Solidi (b)* (2020) 1900538, <http://dx.doi.org/10.1002/pssb.201900538>.
- [28] S. Cortes, et al., Design, manufacture, and Quasi-Static Testing of metallic negative Stiffness Structures within a Polymer Matrix, *Exp. Mech.* 57 (2017) 1–9.
- [29] S. Chen, et al., A novel composite negative stiffness structure for recoverable trapping energy, *Composites A* 129 (2020) 105697, <http://dx.doi.org/10.1016/j.compositesa.2019.105697>.
- [30] X. Tan, et al., Novel multidirectional negative stiffness mechanical metamaterials, *Smart Mater. Struct.* 29 (2020) 015037, <http://dx.doi.org/10.1088/1361-665X/ab47d9>.
- [31] F. Pan, et al., 3D Pixel mechanical metamaterials, *Adv. Mater.* (2019) e1900548, <http://dx.doi.org/10.1002/adma.201900548>.
- [32] S.H. Chan, R.S. Lakes, M.E. Plesha, Design, Fabrication, and analysis of lattice exhibiting energy absorption via Snap-through Behavior, *Mater. Des.* (2018).
- [33] B. Wang, et al., Cushion performance of cylindrical negative stiffness structures: Analysis and optimization, *Compos. Struct.* 227 (2019) 111276, <http://dx.doi.org/10.1016/j.compstruct.2019.111276>.
- [34] C. Morris, L. Bekker, C. Spadaccini, M. Haberman, C. Seepersad, Tunable mechanical metamaterial with constrained negative stiffness for improved Quasi-Static and Dynamic Energy Dissipation, *Adv. Energy Mater.* (2019) 1900163, <http://dx.doi.org/10.1002/adem.201900163>.
- [35] C. Valencia, D. Restrepo, N.D. Mankame, P.D. Zavattieri, J. Gomez, Computational characterization of the wave propagation behavior of multi-stable periodic cellular materials, *Extreme Mech. Lett.* 33 (2019) 100565, <http://dx.doi.org/10.1016/j.eml.2019.100565>.
- [36] J. Meaud, K.K. Che, Tuning elastic wave propagation in multistable architected materials, *Int. J. Solids Struct.* 122 (2017) 69–80, <http://dx.doi.org/10.1016/j.ijsolstr.2017.05.042>.
- [37] T. Chen, O.R. Bilal, K. Shea, C. Daraio, Harnessing bistability for directional propulsion of untethered, soft robots, *Proc. Natl. Acad. Sci.* 115 (2017).
- [38] C.B. Churchill, D.W. Shahan, S.P. Smith, A.C. Keefe, G.P. McKnight, Dynamically variable negative stiffness structures, *Sci. Adv.* 2 (2016) e1500778, <http://dx.doi.org/10.1126/sciadv.1500778>.
- [39] X. Kuang, et al., Advances in 4D Printing: Materials and applications, *Adv. Funct. Mater.* 29 (2019) 1805290, <http://dx.doi.org/10.1002/Adfm.201805290>.
- [40] Z. Zhao, et al., Three-dimensionally printed mechanical metamaterials with thermally tunable Auxetic Behavior, *Phys. Rev. A* 11 (2019) <http://dx.doi.org/10.1103/PhysRevApplied.11.044074>.
- [41] M.A. Wagner, T.S. Lumpe, T. Chen, K. Shea, Programmable, active lattice structures: Unifying stretch-dominated and bending-dominated topologies, *Extreme Mech. Lett.* 29 (2019) 100461, <http://dx.doi.org/10.1016/j.eml.2019.100461>.
- [42] S. Shan, et al., Harnessing multiple folding mechanisms in soft periodic structures for tunable control of Elastic Waves, *Adv. Funct. Mater.* 24 (2015) 4935–4942.
- [43] J.A. Jackson, et al., Field responsive mechanical metamaterials, *Sci. Adv.* 4 (2018) eaau6419, <http://dx.doi.org/10.1126/sciadv.aau6419>.
- [44] B. Florijn, C. Coulais, M. van Hecke, Programmable mechanical metamaterials, *Phys. Rev. Lett.* 113 (2014) 175503, <http://dx.doi.org/10.1103/PhysRevLett.113.175503>.
- [45] Y. Chen, L. Jin, Geometric role in designing pneumatically actuated pattern-transforming metamaterials, *Extreme Mech. Lett.* 23 (2018) 55–66, <http://dx.doi.org/10.1016/j.eml.2018.08.001>.
- [46] B. Moore, T. Jaglinski, D.S. Stone, R.S. Lakes, Negative incremental bulk modulus in foams, *Phil. Mag. Lett.* 86 (2006) 651–659, <http://dx.doi.org/10.1080/09500830600957340>.
- [47] M. Alturki, R. Burgueño, Multistable Cosine-Curved Dome System for Elastic Energy Dissipation, *J. Appl. Mech.* 86 (2019) 091002, <http://dx.doi.org/10.1115/1.4043792>.
- [48] X. Tan, et al., Mechanical response of negative stiffness truncated-conical shell systems: experiment, numerical simulation and empirical model, *Composites B* 188 (2020) 107898, <http://dx.doi.org/10.1016/j.compositesb.2020.107898>.
- [49] A. Eslaminejad, M. Ziejewski, G. Karami, Vibrational properties of a Hemispherical shell with its inner fluid pressure: An inverse method for noninvasive intracranial pressure monitoring, *J. Vib. Acoust.* 141 (2019) <http://dx.doi.org/10.1115/1.4042928>.
- [50] A. Eslaminejad, M. Ziejewski, G. Karami, An experimental-numerical modal analysis for the study of shell-fluid interactions in a clamped hemispherical shell, *Appl. Acoust.* 152 (2019) 110–117, <http://dx.doi.org/10.1016/j.apacoust.2019.03.029>.